Investigating Self-Assembled Multivalent Heparin Binders in Highly Competitive, Biologically Relevant, Aqueous Media

Stephen M. Bromfield,[a,‡] Paola Posocco,[b,c,‡] Ching Wan Chan,[a] Marcelo Calderon,[d] Scott R. Guimond,[e] Jeremy E. Turnbull,[e] Sabrina Pricl,[b,c,] * and David K. Smith*[a]

[a] Department of Chemistry, University of York, Heslington, York, YO10 5DD, UK. Fax: +44 (0)1904 324516. E-mail: david.smith@york.ac.uk

[b] Simulation Engineering (MOSE) Laboratory, Department of Engineering and Architecture (DEA), University of Trieste, 34127, Trieste, Italy

[c] National Interuniversity Consortium for Material Science and Technology (INSTM), Research Unit MOSE-DEA, University of Trieste, 34127 Trieste,

[d] Institut for Chemie and Biochemie, Freie Universität Berlin, Takustrasse 3, D-14195 Berlin, Germany.

[e] Institute of Integrative Biology, Biosciences Building, University of Liverpool, Crown Street, Liverpool L69 7ZB, UK.

‡These authors equally contributed to this work *SP corresponding author (molecular modeling)

SUPPORTING INFORMATION

Contents

1 Assay Methods & Notes

All materials employed in the following assays were obtained from commercial sources and used without further purification unless otherwise stated. Sodium salt heparin from porcine intestinal mucosa with a molecular weight of 15,000 ± 2,000 Da (192 IU mg^{-1}) was obtained from Calbiochem®. Protamine sulfate salt from salmon (Grade X, amorphous powder), PAMAM dendrimers, Trizma® hydrochloride (Tris HCl) and Human Serum (from human male AB plasma) were obtained from Sigma Aldrich. Compounds **C22-G1** and Mallard Blue (MalB) was prepared as previously described[1,2] and MalB was stored in the dark. UV/Vis absorbance was measured on a Shimadzu UV-2401PC spectrophotometer, fluorescence on a Hitachi F-4500 spectrofluorimeter, and mass spectrometric analysis was carried out using a Bruker Daltonics Micro-TOF mass spectrometer. All experiments were performed in triplicate unless otherwise stated.

For the purpose of calculations, the molecular weight of heparin is assumed as that of the sodiated analogue of the heparin repeat unit shown in Figure 1: namely 665.40 g mol^{-1}, anf four anionic charges are assumed per repeat unit. It should be noted that as supplied, heparin only contains ca. 30-40% of material with the active sequence of repeat units. However, all the sample contains anionic saccharide units which can bind to cationic species, even if they are in the wrong sequence. Hence to best evaluate binding concentrations and charge efficiencies, we report the total concentration of the anionic disaccharide – irrespective of whether it is present in the active form of heparin or not. However, all presented data which refers to the 'dose' of binders (in mg/units) refers to their ability to bind only the specific clinically active heparin.

2 Heparin-Mallard Blue Displacement Assay

2.1 In buffer[2]

A cuvette containing 2 mL of MalB (25 μM), heparin (27 μM) and NaCl (150 mM) in Tris HCl (10 mM) was titrated with binder stock solution to give the cuvette a suitable binder-heparin charge ratio. The binder stock solution was composed of the original MalB/heparin/NaCl/Tris HCl stock solution endowed additionally with a concentration of

binder such that, after addition of 10 μL binder stock, the cuvette charge ratio (+ : –) is 0.1. After each addition, the cuvette was inverted to ensure good mixing and the absorbance at 615 nm was recorded against a Tris HCl (10 mM) baseline. A normalisation range for absorption was set against a solution of MalB (25 μM), NaCl (150 mM) in Tris HCl (10 mM) and one containing MalB (25 μM), heparin (27 μM), NaCl (150 mM) in Tris HCl (10 mM).

2.2 In Serum[2]

Fourteen cuvettes were charged with 1.75 mL of MalB (28.53 μM) in Tris HCl (10 mM) and a volume of binder stock solution to give the cuvette a suitable binder-heparin charge ratio. The binder stock solution was additionally endowed with its own MalB (25 μM), heparin (27 μM) and Tris HCl (10 mM) concentrations. The concentration of binder in the binder stock was determined in the same manner described for the heparin displacement assay in buffer. Separately, a heparin (216 μM) solution was made in 100% human serum. Sequentially, each cuvette was titrated with 0.25 mL of the heparin-in-serum solution and inverted to ensure thorough mixing. The absorbance was recorded at 615 nm against a baseline of (1.75 mL 10 mM Tris HCl, 0.25 mL 100% Human Serum) and a normalisation range for absorption was set against a solution containing exclusively MalB (25 μM) and one containing MalB (25 μM) and heparin (27 μM).

2.3 In 0 – 10% Human Serum

A range of cuvettes were charged with 1.75 mL of MalB (28.53 μM) in Tris HCl (10 mM) and a volume of binder stock solution to give the cuvette a binder-heparin charge ratio of 0.67 after all components had been added. The binder stock solution was additionally endowed with its own MalB (25 μM), heparin (27 μM) and Tris HCl (10 mM) concentrations. Separately, a range of human serum stock solutions (0 – 10%) were made by dilution of human serum with Tris HCl (10 mM) before each was endowed with heparin (216 μM). Sequentially, each cuvette was titrated with 0.25 mL of one of the heparin-in-serum solutions and inverted to ensure thorough mixing. The absorbance was recorded at 615 nm against a baseline of (1.75 mL 10 mM Tris HCl, 0.25 mL 5% Human Serum) and a normalisation range for absorption was set against a solution containing exclusively MalB (25 μM) and one containing MalB (25 μM) and heparin (27 μM).

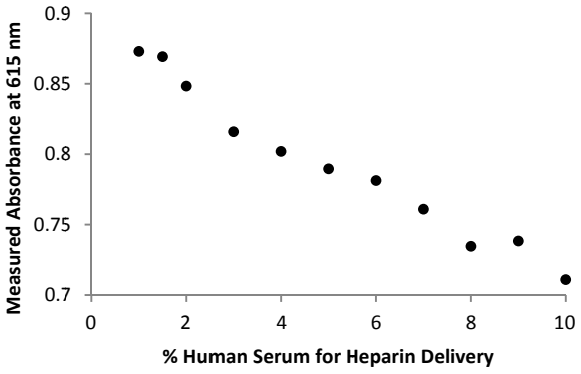

Fig. S1. Effect of increasing amounts of serum on the interaction between **C22-G1**, heparin and MalB, measuring absorbance of MalB at 615 nm using a charge excess of 0.67 (**C22-G1**/Heparin).

3 Mass Spectrometric Degradation Study

The binder was dissolved (200 µM) in ammonium carbonate (10 mM, pH 7.5). 250 µL of this binder solution was combined with 250 µL of a Gly-Ala standard (1 mM, in 10 mM ammonium carbonate) for mass spectrometric analysis. Following incubation of the binder solution for 24 hours at 37°C, the same analysis was repeated. The identity of species detected in this study are shown in Figure S2 while individual spectra of the binder sample at 0 hours and 24 hours are shown in Figure S3 and Figure S4 respectively.

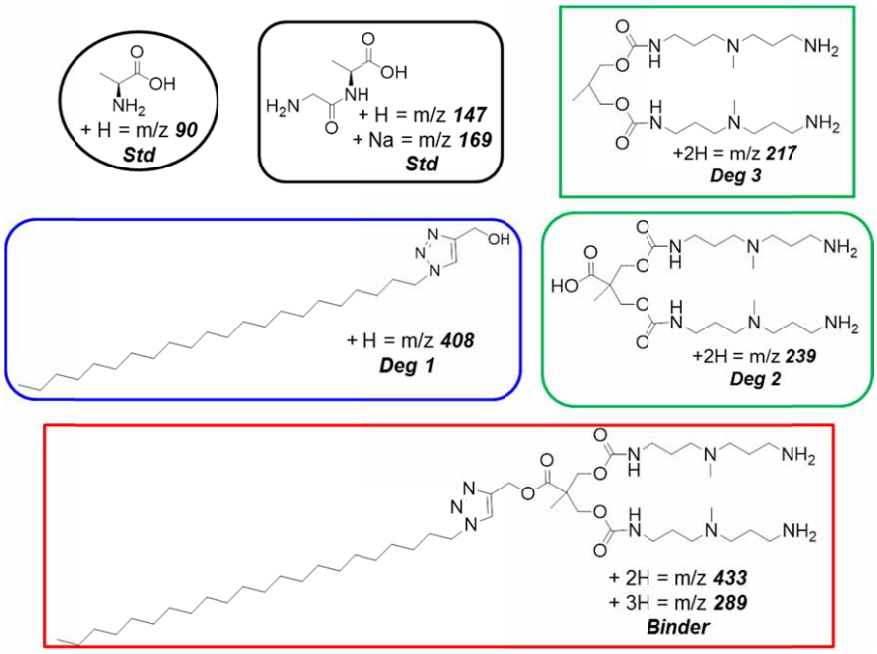

Figure S2 – Molecular species identified in mass spectrometric analysis

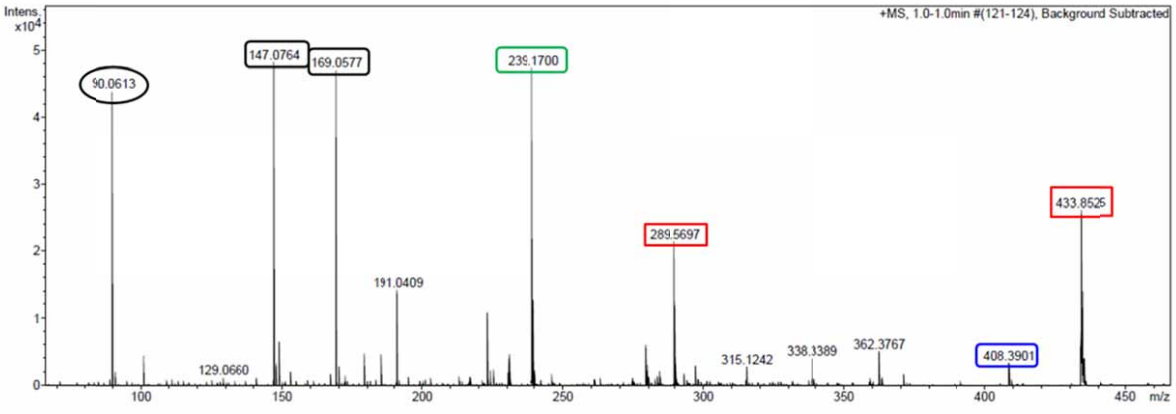

Figure S3 – Mass spectrum of binder in the presence of internal standard at 0 hours

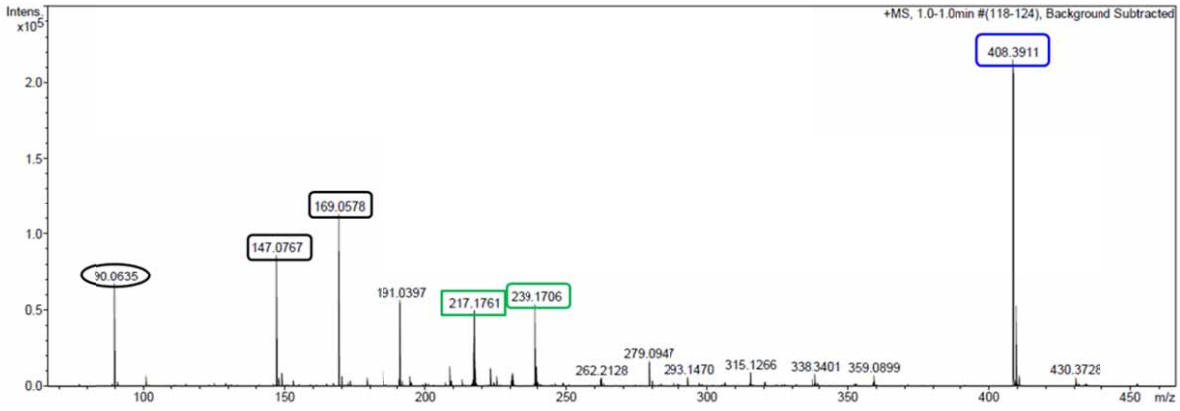

Figure S4 – Mass spectrum of binder in the presence of internal standard following incubation at 37°C for 24 hours

4 Fluorescence-based Degradation Study

The binder was dissolved in phosphate buffered saline (PBS, 0.01 M, endowed with NaCl (138 µM) and KCl (2.7 µM)) at a concentration of 25 µM. In a cuvette, an aliquot (1 mL) of this solution was mixed with a small amount of Nile Red (1 µL, 2.5 mM in ethanol). Following inversion to ensure mixing, fluorescence intensity at 635 nm was recorded using a 550 nm excitation wavelength. The binder stock solution was incubated at 37°C for 24 hours before another aliquot (1 mL) was taken for fluorescence measurement as before. In the time resolved experiment, the initial solution was left in the fluorimeter and the emission was monitored at regular time periods. For the degradation experiment in the presence of heparin, the binder stock solution was additionally endowed with a heparin concentration corresponding to a dosage of 0.79 mg / 100IU.

5 Dynamic Light Scattering (DLS)

The micelle characteristics were determined using a Zetasizer Nano (Malvern Instruments Ltd., Worcestershire, UK). In brief, the principle is based on the measurement of the backscattered light fluctuations at an angle of 173° and the calculation of an autocorrelation function. The samples were measured undiluted at 25ºC and adjusted to this temperature for 2 minutes prior to the measurement. The autocorrelation functions were analysed using the DTS v5.1 software provided by Malvern. Measurements were done in triplicate with 15–20 runs per single measurement and the calculated mean values (based in intensity distribution) were used. All measurements were carried out at 25°C using folded capillary cells (DTS 1060) as triplicate.

Dendron solutions were freshly prepared by dissolving an appropriate amount of dry polymer (5 mg/mL) in the filtered Tris.HCl 10 mM buffer solution. The sample solutions were then stirred thoroughly to ensure proper mixing and dissolution prior to measurement. The values allowed determination of micelle diameters according to the intensity distribution. Mixtures of dendrons in Tris.HCl 10mM and NaCl 150 mM with heparin and/or albumin were performed at different ratios and incubated for 10 min at 25 °C prior to the measurement.

TrisCl+NaCl 10 mM

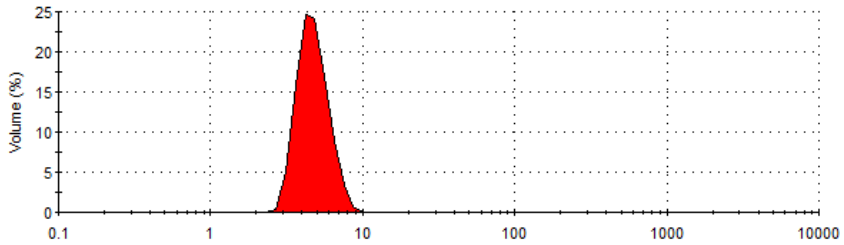

TrisCl+NaCl 150 mM

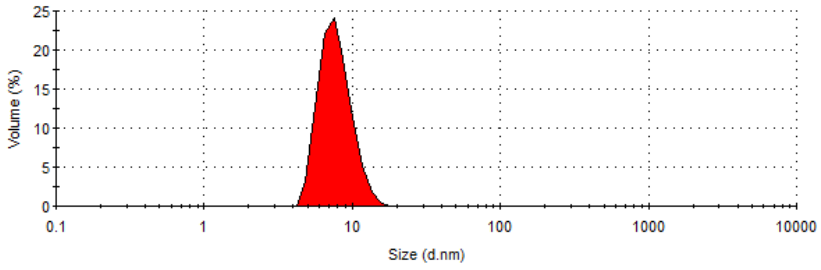

6 Clotting Assays

Clotting studies employed an Axis Shield Thrombotrack coagulation analyser in conjunction with Behnk Elektronik cuvettes and ball bearings. Technoclone normal citrated plasma (re-suspended in HPLC grade water), Acros Organics calcium chloride (50 mM in HPLC grade water), Celsus porcine mucosal heparin (201 IU mg^{-1}), Siemens Thromborel® S (re-suspended in HPLC grade water at double the manufacturers recommended concentration) and Siemens Pathromtin SL (inverted 8 times prior to use).

6.1 Prothrombin Time (PT Assay)

A cylindrical cuvette, pre-warmed to 37°C on a heating block, was placed in the coagulation analyser and charged with a ball bearing and normal citrated plasma (50 µL). Following incubation for at least 1 minute, pre-warmed (37°C) test sample (50 µL) was added along with Thromborel® S reagent (50 µL). Upon addition of the final reagent, the coagulation analyser was initiated. Clotting times are reported as the time at which the coagulometer was no longer able to stir the sample. Samples remaining unclotted after 120 seconds were recorded as 'no clot.' All measurements were carried out in triplicate with error values reported as one standard deviation.

6.2 Activated Partial Thromboplastin Time (aPTT Assay)

A cylindrical cuvette, pre-warmed to 37°C on a heating block, was placed in the coagulation analyser and charged with a ball bearing, normal citrated plasma (50 µL), Pathromtin SL (50 µL) and test sample (25 µL). Following incubation for at least 2 minutes, pre-warmed (37°C) calcium chloride (25 µL) was added and the coagulation analyser was initiated. Clotting times are reported as the time at which the coagulometer was no longer able to stir the sample. Samples remaining unclotted after 120 seconds were recorded as 'no clot.' All measurements were carried out in triplicate with error values reported as one standard deviation.

7 Computational Methods

7.1 Multiscale modeling of C22-G1 self-assembling process

In this work, we resorted to our well-validated multiscale molecular modeling procedure[3,4-7] based on the systematic elimination of computationally expensive degrees of freedom while retaining implicitly their influence on the remaining degrees freedom in the mesoscopic model. Accordingly, using the information obtained from atomistic molecular dynamics simulation (MD), we parameterized the dissipative particle dynamics (DPD)[8] models that incorporate all essential physics/phenomena observed at the finer level.

The outline of the general strategy of our multiscale modeling approach may be summarized as follows: i) explicit solvent atomistic MD calculations[9] were performed on **C22-G1** and its assembly at two ionic strengths (i.e., 150 mM and 0 mM); ii) the mesoscale model parameters were calculated exploiting the conformational properties and energetic values obtained from MD simulation at point (i)[10] using an explicit solvent model in which each dendron was represented as single force centers (beads) and solvent was treated explicitly in the presence of ions and counterions. Langevin dynamics were then conducted using the DPD representation of the system; iii) the equilibrium configurations of the self-assembled systems obtained at point (ii) were mapped back to the corresponding atomistic MD models, and then new atomistic MD simulations were conducted to calculate binding energies between each micelle and the heparin molecule under high salt/ no salt conditions.[3]

7.2 Atomistic molecular dynamics simulation of C22-G1 compound and its assembly in high salt/ no salt conditions

All atomistic simulations and data analysis were performed with the AMBER 11 suite of programs.[11] A **C22-G1** compound model was built and geometry-optimized using the Antechamber module of AMBER 11 and the GAFF force field.[12] The dendron structure was solvated in a TIP3P[13] water box to generate a bulk system with concentration lower than the corresponding experimental CAC value. Then, the required amount of Na^+ and Cl^- ions were added to neutralize the system and to mimic high salt/no salt conditions, removing eventual overlapping water molecules. The solvated molecules were subjected to a combination of steepest descent/conjugate gradient minimization of the potential energy, during which all

bad contacts were relieved. The relaxed systems were then gradually heated to 300 K in three intervals by running constant volume-constant temperature (NVT) MD simulation, allowing a 0.5 ns interval per 100 K. Subsequently, 10 ns MD simulations under isobaric-isothermal (NPT) conditions were conducted to fully equilibrate each solvated compound. The *SHAKE* algorithm[14] with a geometric tolerance of 5×10^{-4} Å was imposed on all covalent bonds involving hydrogen atoms. Temperature control was achieved using the Langevin[15] temperature equilibration scheme and an integration time step of 2 fs. At this point, these MD runs were followed by other 10 ns of NVT MD and 10 ns of NVT data collection runs. The particle mesh Ewald (PME) method[16] was used to treat the long-range electrostatics. To calculate interaction energies and conformational properties, 1000 snapshots were saved during the MD data collection period described above, one snapshot per 10 ps of MD simulation.

Exploiting the morphological information obtained at the mesoscale level (*vide infra*), the corresponding atomistic models of **C22-G1** micelles were built and placed in a cubic box filled with water molecules extending at least 20 Å from the solute. A suitable number of Na^+ and Cl^- ions was added to neutralize the system and to mimic ionic strength (150 mM and 0 mM). The supramolecular assembly was relaxed according to the procedure described above, followed by 40 ns of NVT MD.

All of the production molecular dynamics simulations were carried out working in parallel on IBM FERMI and Eurora calculation cluster of the CINECA supercomputer centre (Bologna, Italy).

7.3 Background theory of mesoscopic Dissipative Particle Dynamics (DPD) simulations

DPD is a particle-based mesoscale technique first introduced by Hoogerbrugge and Koelman[8b] and cast in its present form by Español and Warren,[17] and Groot and Warren.[8a] In DPD, a number of particles are coarse-grained into fluid elements, called beads. These DPD beads interact via pairwise additive interactions that locally conserve momentum, a necessary condition for a correct description of hydrodynamics, while retaining essential information about the structural and physical-chemical properties of the system components. An advantageous feature of DPD is that it employs soft repulsive interactions between the beads,

thereby allowing for larger integration time steps than in a typical molecular dynamics using for example Lennard-Jones interactions. Thus, time and length scales much larger (up to microseconds range) than those in atomistic molecular dynamics simulations can be accessed.

In DPD the beads move according to Newton's equations of motion:

$$d\boldsymbol{r}_i(t) / dt = \boldsymbol{p}_i(t) / m_i \quad \text{(SI1)}$$

$$d\boldsymbol{p}_i(t) / dt = \boldsymbol{f}_i(t) \quad \text{(SI2)}$$

where $\boldsymbol{r}_i(t)$, $\boldsymbol{p}_i(t)$, m_i, and $\boldsymbol{f}_i(t)$ are the position, momentum, mass and net force of particle i, respectively. $\boldsymbol{f}_i(t)$ is given as the sum of three different forces: a conservative force $\boldsymbol{F}_{ij,C}$, a dissipative force $\boldsymbol{F}_{ij,D}$, and a random force $\boldsymbol{F}_{ij,R}$:

$$\boldsymbol{f}_i(t) = \Sigma_{i \neq j} \boldsymbol{F}_{ij,C} + \boldsymbol{F}_{ij,D} + \boldsymbol{F}_{ij,R} \quad \text{(SI3)}$$

All forces are pairwise and lay along the line joining two interacting particles i and j. The conservative force for non-bonded beads $\boldsymbol{F}_{ij,C}$ represents a soft repulsion modeled as a linear function of the distance between two particles, while the dissipative force $\boldsymbol{F}_{ij,D}$ slows down the particle motions, thus accounting for the effects of viscosity, and the random force $\boldsymbol{F}_{ij,R}$ provides the thermal or vibrational energy of the system. The dissipative force acts to reduce the relative momentum between beads i and j, while random force $\boldsymbol{F}_{ij,R}$ impels energy into the system. The expressions for the forces are given by the following equations:

$$\boldsymbol{F}_{ij,C} = a_{ij} (1 - r_{ij} / r_c) \times \boldsymbol{r}_{ij} / r_{ij} \quad \text{(SI4)}$$

$$\boldsymbol{F}_{ij,D} = -\gamma_{ij} \omega^D(r_{ij}) [(\boldsymbol{r}_{ij} / r_{ij}) \times \boldsymbol{v}_{ij}] (\boldsymbol{r}_{ij} / r_{ij}) \quad \text{(SI5)}$$

$$\boldsymbol{F}_{ij,R} = \sigma_{ij} \omega^R(r_{ij}) (\zeta_{ij} / \Delta t^{0.5}) (\boldsymbol{r}_{ij} / r_{ij}) \quad \text{(SI6)}$$

where a_{ij} is the maximum repulsion parameter between particle i and j, $\boldsymbol{r}_{ij} = \boldsymbol{r}_i - \boldsymbol{r}_j$ is the vector joining beads i and j, $r_{ij} = |\boldsymbol{r}_{ij}|$ is the distance between particle i and j, $\boldsymbol{v}_{ij} = \boldsymbol{v}_i - \boldsymbol{v}_j$ is the relative velocity, and $\boldsymbol{v}_i = \boldsymbol{p}_i / m_i$. All the above forces act within the cut-off radius r_c, which basically constitutes the length scale of the entire system. γ_{ij} is a friction coefficient, σ_{ij} the noise amplitude, ζ_{ij} a Gaussian random number with a zero mean and a unit variance chosen independently for each pair of particles, and Δt is the time step in the simulation. $\omega^D(r_{ij})$ and $\omega^R(r_{ij})$ are weight functions vanishing for distance greater than r_c.

In DPD, molecules are built by tying beads together using Hookean springs with the potential given by:

$$U_{bb}(i, i+1) = \frac{1}{2} k_{bb} (r_{i,i+1} - l_0)^2 \quad \text{(SI7)}$$

where i, $i+1$ label adjacent beads in the molecule. The spring constant, k_{bb}, and unstretched length l_0, are chosen so as to fix the average bond length to a desired value. Chain stiffness is modeled by a three body potential acting between adjacent bead triples in a row using equation (SI8):

$$U_{bbb}(i-1,i,i+1) = k_{bbb} (1-\cos (\phi - \phi_0)) \quad \text{(SI8)}$$

in which the angle ϕ is defined by the scalar product of the two bonds connecting the pair of adjacent beads $i-1$, i, and $i+1$.

Furthermore, in order to correctly derive the electrostatic interactions between charged beads (i.e. present on the dendrons and ions), the electrostatic force F_{ij}^{E} between two charged beads i and j is analysed following the approach reported in Groot's work.[18] According to this study, the electrostatic field is solved by smearing the charges over a lattice grid, the size of which is determined by a balance between the fast implementation and the correct representation of the electrostatic field.

7.4 DPD modeling of C22-G1 self-assembly

We modelled the different compounds at a coarse-grained level using branched and flexible amphiphilic chains made up of 4 bead types: one hydrophilic charged bead H, as the terminal charged repeating unit of the dendron, one hydrophobic building block C, representing the alkyl chain, two further bead types, L1 and L2, linking the hydrophilic and hydrophobic parts together. Comparing the appropriate MD and DPD pair-pair correlation functions, we determined the mesoscale topology of **C22-G1**.[3,5,10b,10d,10f,19] The coarse-grained model obtained for this compound is shown in Figure S5.

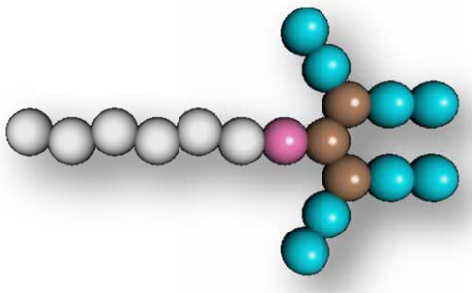

Figure S5. Schematic representation of the coarse-grained DPD models of **C22-G1**. The colours of the beads stand for hydrophilic dendron beads H (light blue), alkyl tail beads C (white), linker beads L1 (pink), and L2 (brown).

Solvent molecules were simulated by single bead types W, and an appropriate number of counterions of a charge of ± 1 were added to preserve charge neutrality and to account for the two experimental solution ionic strengths. All simulations were performed in a 3D-periodic cubic box. The appropriate number of **C22-G1** molecules was added to the simulation box in order to fit experimental concentrations. Approximately 8×10^6 time steps at 300 K were performed in each DPD run, thus corresponding to a total physical time for each calculation of about 3 μs.

The intra- and intermolecular interactions between DPD particles are expressed by the conservative parameter a_{ij}, defined by equation (SI4). This quantity accounts for the underlying chemistry of the system considered. In this work, we employed a well-validated strategy that correlates the interaction energies estimated from atomistic molecular dynamics simulations[20] to the mesoscale a_{ij} parameter values.[3,10,21] Following and adapting this computational recipe to the present case, the interaction energies between the solvated molecules estimated using the MD-based procedure described above were rescaled onto the corresponding mesoscale segments. The bead-bead interaction parameter for water was set equal to $a_{ww} = 25$ in agreement with the correct value of DPD density $\rho = 3$.[8a] The maximum level of hydrophobic/hydrophilic repulsion was captured by setting the interaction parameter a_{ij} between the water bead W and the alkyl tail bead C as 79 (70 in the case of no salt). The counterions were set to have the interaction parameters of water.[22] Once these parameters were assigned, all the remaining bead-bead interaction parameters for the DPD simulations were easily obtained, starting from the atomistic interaction energies values, as described in

our previous works.[3,10f] The entire set of DPD interaction parameters employed in this work is summarized in Table 1.

Table S1. DPD bead-bead interaction parameters obtained for **C22-G1** in water under high salt (left) and no salt (right) conditions.

a_{ij}	*H*	*L1*	*L2*	*C*	*W*
	41	36	32	78	21
L1	36	25	33	45	29
L2	32	33	25	47	32
C	78	45	47	25	79
W	21	29	32	79	25

a_{ij}	*H*	*L1*	*L2*	*C*	*W*
H	62	41	35	80	20
L1	41	25	30	41	27
L2	35	30	25	46	30
C	80	41	46	25	70
W	20	27	30	70	25

7.5 Atomistic molecular dynamics simulations of C22-G1 dendron micelle, G2-PAMAM and protamine in high salt/ no salt conditions

The optimized models of G2-PAMAM dendrimer, protamine, and heparin were taken from our previous works.[2,9c] The model system of **C22-G1** micelle was taken from an equilibrated configuration of the assembly at two ionic strengths, removing all water molecules and ions.

The complex of heparin with **C22-G1** micelle, G2-PAMAM dendrimer, and protamine was achieved by adapting a consolidated procedure developed by our group.[9,23] Accordingly, it will be reported here briefly. To build the 3D models of the complexes, the heparin chain was initially placed close to each micelle/molecule periphery. The resulting molecular pair was subsequently energy minimized to yield a starting structure devoid of substantial van der Waals overlaps. Each complex was then solvated with an appropriate number of TIP3P[13] water molecules extending at least 20 Å from the solute. A suitable number of Na^+ and Cl^- counterions were added to neutralize the system and to mimic high salt/no salt conditions (i.e. 150 mM and 0 mM). Eventual overlapping water molecules were removed. Each complex molecular model was then subjected to a combination of steepest descent and conjugate gradient energy minimization steps (50000 cycles), in order to relax close atomic distances. The energy-minimized systems were further equilibrated by performing 4 to 12 ns MD

simulations in the NPT ensemble using an integration step of 1fs. During equilibration, different energetic components as well as static and conformational properties were monitored, to ensure their stabilization prior to production runs. MD production runs were performed on equilibrated systems again in the NPT ensemble with 1 fs time step (T = 300 K, P = 1 bar). The Langevin method for the control of temperature (with a damping coefficient of 5 ps^{-1}) and the Nose-Hoover Langevin piston method[24] for the control of pressure (using a piston period of 0.8 ps and a decay time of 0.4 ps) were employed for temperature and pressure control, respectively. Electrostatic interactions were computed by means of the PME algorithm[14]. Depending on the molecular dimensions of the examined systems, production MD trajectories of 10 to 50 ns were generated. For the calculation of the binding free energy between heparin and each compound, 4000 snapshots were saved during the MD data collection period described above, one snapshot per each 10 ps of MD simulation.

All of the production (MD) simulations were carried out using AMBER 11 platform and the *ff03* all-atom force field by Duan et al.[25] working in parallel on IBM FERMI and Eurora calculation cluster of the CINECA supercomputer center (Bologna, Italy). All energetic analyses were performed by running the MM/PBSA script supplied with AMBER 11 on a single MD trajectory of each complex considered.

To estimate the free energy of binding ΔG_{bind} between each compound (**C22-G1** micelle, G2-PAMAM, and protamine) and the heparin molecule, we resorted to a well-established computational recipe[9] based on the so-called Molecular Mechanics/Poisson-Boltzmann Surface Area (MM/PBSA) methodology.[26] Briefly, for a non-covalent association of two molecular entities A + B → AB, the free energy of binding involved in the process may be generally written as $\Delta G_{bind} = G_{AB} - G_A - G_B$. For any species on the right hand side of this equation, from basic thermodynamics we have $G_i = H_i - TS_i$, where H_i and S_i are the enthalpy and entropy of the i-th species, respectively and T is the absolute temperature. In view of this expression, ΔG_{bind} can then be written as: $\Delta G_{bind} = \Delta H_{bind} - T\Delta S_{bind}$. ΔH_{bind} is the variation in enthalpy upon association and, in the MM/PBSA framework of theory, can be calculated by summing the molecular mechanics energies (ΔE_{MM}) and the solvation free energy (ΔG_{solv}), i.e., $\Delta H_{bind} = \Delta E_{MM} + \Delta G_{solv}$. ΔE_{MM} in turn is obtained from a single MD trajectory of the molecular complex as $\Delta E_{MM} = \Delta E_{vdW} + \Delta E_{ele}$, where ΔE_{vdW} is the variation of the nonbonded van der Waals energy and ΔE_{ele} is the electrostatic contribution calculated from the Coulomb

potential. The solvation term ΔG_{solv} is given by $\Delta G_{solv} = \Delta G_{pol} + \Delta G_{np}$, in which ΔG_{pol} is obtained by solving the Poisson-Boltzmann equation and ΔG_{np} is the nonpolar solvation term estimated via the semiempirical expression: $\Delta G_{np} = \gamma \times SASA + \beta$, in which SASA is the solvent accessible surface area of the molecule, γ is the surface tension parameter (0.00542 kcal/Å^2/mol), and β = 0.92 kcal/mol. Finally, the estimation of the entropic contribution – $T\Delta S_{bind}$ is performed using normal mode analysis, which requires the computation of eigenvectors and eigenvalues via the diagonalization of the Hessian matrix.

We deconvoluted the enthalpic term of the *effective* free energy of binding into its main components for each individual *effective* (i.e., contributing actively to the binding) charged residues (RESC) of G2-PAMAM and C22-G1 in complex with heparin under different salt conditions (Table S2). This allowed us to determine the relative contribution of electrostatic binding and dispersion interactions to the overall binding event, and hence determine the dominant factors controlling the response of binding to the presence of physiological salt conditions.

Finally, the effective number of charges involved in binding, and the corresponding effective free energy of binding values (main text, Table 3) were obtained performing a *per residue binding free energy decomposition* (PRBFED) exploiting the MD trajectory of each given heparin complex. This analysis was carried out using the MM/GBSA approach,[27] and was based on the same snapshots used in the binding free energy calculation.

Table S2. Deconvolution of the enthalpic term of the *effective* free energy of binding into its main components for each individual *effective* (i.e., contributing actively to the binding) charged residues (RESC) of G2-PAMAM and C22-G1 in complex with heparin under different salt conditions. All energies are in kcal/mol. Data standard deviations are in the range of ±0.01 ÷ ±0.03 kcal/mol.

150 mM NaCl

G2-PAMAM						C22-G1					
[a]RESC	[b]ΔE_{vdw}^{eff}	[c]ΔE_{ele}^{eff}	[d]ΔG_{GB}^{eff}	[e]ΔG_{np}^{eff}	[f]ΔH^{eff}	RESC	ΔE_{vdw}^{eff}	ΔE_{ele}^{eff}	ΔG_{GB}^{eff}	ΔG_{np}^{eff}	ΔH^{eff}
1	-0.54	-45.68	44.64	-0.09	-1.67	1	-2.60	-115.26	108.60	-0.12	-9.38
2	-0.31	-39.70	37.99	-0.05	-2.07	2	-1.63	-97.42	92.18	-0.08	-6.94
3	-0.50	-47.04	46.25	-0.08	-1.37	3	0.39	-86.60	81.02	-0.01	-5.20
4	-0.27	-44.03	42.88	-0.05	-1.46	4	-0.81	-103.65	98.43	-0.06	-6.08
5	-0.42	-44.48	43.17	-0.05	-1.79	5	-0.51	-104.51	99.24	-0.05	-5.83
6	-0.37	-40.08	38.49	-0.05	-2.01	6	-1.07	-99.54	94.69	-0.06	-5.97
7	-0.27	-43.85	42.21	-0.04	-1.95	7	-0.20	-89.78	85.60	-0.04	-4.42
8	-0.32	-41.20	39.82	-0.05	-1.75	8	-1.99	-85.77	82.42	-0.05	-5.40
9	-0.30	-42.86	42.04	-0.05	-1.16	9	-1.67	-87.85	83.76	-0.03	-5.78
10	-0.24	-45.88	44.76	-0.02	-1.37	10	-1.43	-107.68	103.69	-0.05	-5.47
11	-0.51	-41.61	40.42	-0.07	-1.76	11	-3.73	-93.53	90.89	-0.10	-6.47
12	-0.51	-40.67	39.53	-0.08	-1.74	12	-0.66	-81.21	77.71	-0.05	-4.21
13	-0.28	-40.62	39.43	-0.08	-1.56	13	-0.44	-89.36	85.61	-0.04	-4.23
Σ	**-4.84**	**-557.70**	**541.63**	**-0.76**	**-21.67**	14	-0.33	-79.48	76.13	-0.03	-3.70
						15	-0.23	-79.32	76.00	-0.03	-3.58
						16	-2.23	-85.80	82.87	-0.05	-5.21
						Σ	**-19.13**	**-1486.75**	**1418.82**	**-0.83**	**-87.89**

0 mM NaCl

G2-PAMAM						C22-G1					
RESC	ΔE_{vdw}^{eff}	ΔE_{ele}^{eff}	ΔG_{GB}^{eff}	ΔG_{np}^{eff}	ΔH^{eff}	RESC	ΔE_{vdw}^{eff}	ΔE_{ele}^{eff}	ΔG_{GB}^{eff}	ΔG_{np}^{eff}	ΔH^{eff}
1	-0.30	-54.18	52.29	-0.06	-2.26	1	-1.52	-130.51	128.73	-0.04	-3.34
2	-0.29	-50.84	48.99	-0.04	-2.18	2	-1.63	-143.27	139.49	-0.06	-5.46
3	-0.38	-51.27	49.71	-0.07	-2.01	3	-0.58	-139.51	135.56	-0.03	-4.56
4	-0.40	-46.41	44.78	-0.06	-2.09	4	-2.05	-136.14	129.67	-0.03	-8.56
5	-0.69	-46.54	45.46	-0.06	-1.82	5	-0.99	-140.78	137.10	-0.03	-4.69
6	-0.39	-53.69	51.62	-0.05	-2.50	6	-1.55	-133.31	131.98	-0.03	-2.92
7	-0.33	-43.56	42.45	-0.06	-1.50	7	-2.23	-130.53	127.21	-0.07	-5.63
8	-0.45	-43.85	41.83	-0.04	-2.52	8	-0.61	-118.13	115.57	-0.01	-3.17
9	-0.85	-47.53	46.50	-0.11	-2.00	9	-0.17	-108.23	101.61	0.00	-6.79
10	-0.51	-43.93	42.88	-0.06	-1.61	**Σ**	**-11.32**	**-1180.41**	**1146.92**	**-0.31**	**-45.12**
11	-0.30	-44.00	42.44	0.00	-1.86						
12	-0.30	-47.82	47.42	-0.03	-0.73						
13	-0.26	-44.02	43.54	-0.01	-0.76						
14	-0.67	-46.99	46.36	-0.11	-1.41						
15	-0.59	-43.01	41.27	-0.06	-2.40						
Σ	**-6.71**	**-707.64**	**687.53**	**-0.82**	**-27.64**						

[a]RESC represents the aminopropyl-methylamine charged moiety; [b]ΔE_{vdw}^{eff} represents the effective van der Waals interaction energy; [c]ΔE_{ele}^{eff} represents the effective electrostatic interaction energy; [d]ΔG_{GB}^{eff} is the effective Generalized Boltzmann solvation term; [e]ΔG_{np}^{eff} is the effective nonpolar solvation term; [f]ΔH^{eff} is the effective enthalpic term.

8 References

1. A. C. Rodrigo, A. Barnard, J. Cooper, D. K. Smith, *Angew. Chem. Int. Ed.* 2011, **50**, 4675-4679.
2. S. M. Bromfield, P. Posocco, M. Fermeglia, S. Pricl, J. Rodríguez-López and D. K. Smith, *Chem. Commun.* 2013, **49**, 4830-4832.
3. S. M. Bromfield, A. Barnard, P. Posocco, M. Fermeglia, S. Pricl and D. K. Smith, *J. Am. Chem. Soc.*, 2013, **135**, 2911-2914.
4. P. Posocco, E. Laurini, V. Dal Col, D. Marson, K. Karatasos, M. Fermeglia and S. Pricl, *Curr. Med. Chem.* 2012, **19**, 5062-5087.
5. X. Liu, J. Wu, M. Yammine, J. Zhou, P. Posocco, S. Viel, C. Liu, F. Ziarelli, M. Fermeglia, S. Pricl, G. Victorero, C. Nguyen, P. Erbacher, J. P. Behr and L Peng, *Bioconjugate Chem.* 2011, **22**, 2461-2473.
6. S. P. Jones, N. P. Gabrielson, C. H. Wong, H. F. Chow, D. W. Pack, P. Posocco, M. Fermeglia, S. Pricl and D. K. Smith, *Mol. Pharmaceutics* 2011, **8**, 416429.
7. P. Posocco, S. Pricl, S. P. Jones, A. Barnard and D. K. Smith, *Chem. Sci.* 2010, **1**, 393-404.
8. (a) R. D. Groot and P. B. Warren, *J. Chem. Phys.* 1997, **107**, 4423-4435. (b) P. J. Hoogerbrugge and J. M. V. A. Koelman, *Europhys. Lett.* 1992, **19**, 155-160.
9. (a) X. Liu, C. Liu, E. Laurini, P. Posocco, S. Pricl, F. Qu, P. Rocchi and L. Peng, *Mol. Pharmaceutics* 2012, **9**, 470-481. (b) K. Karatasos, P. Paola, E. Laurini and S. Pricl, *Macromol Biosci.* 2012, 12, 225-240. (c) G. M. Pavan, P. Paola, A. Tagliabue, M. Maly, A. Malek, A. Danani, E. Ragg, C. V. Catapano and S. Pricl, *Chem. Eur. J.* 2010, **16**, 7781-7795. (d) S. P. Jones, G. M. Pavan, A. Danani, S. Pricl and D. K. Smith, *Chem. Eur. J.* 2010, **16**, 4519-3245. (e) G. M. Pavan, A. Danani, S. Pricl, D. K. Smith, *J. Am. Chem. Soc.* 2009, **131**, 9686-9694.
10. (a) P. Posocco, C. Gentilini, S. Bidoggia, A. Pace, P. Franchi, M. Lucarini, M. Fermeglia, S. Pricl and L. Pasquato, *ACS Nano* 2012, **6**, 7243-7253. (b) R. Toth, F. Santese, S. P. Pereira, D. R. Nieto, S. Pricl, M. Fermeglia and P. Posocco, *J. Mater. Chem.* 2012, **22**, 5398-5409. (c) P. Posocco, Z. Posel, M. Fermeglia, M. Lisal and S. Pricl, *J. Mater. Chem.* 2010, **20**, 10511-10520. (d) G. Scocchi, P. Posocco, J. W. Handgraaf, J. G. Fraaije, M. Fermeglia and S. Pricl, *Chem. Eur. J.* 2009, **15**, 7586-7592. (e) M. Maly, P. Posocco, S. Pricl and M. Fermeglia, *Ind. Eng. Chem. Res.* 2008,

47, 5023-5038. (f) G. Scocchi, P. Posocco, M. Fermeglia and S. Pricl, *J. Phys. Chem. B* 2007, **111**, 2143-2151.

11. D. A. Case, T. A. Darden, T. E. Cheatham III, C. L. Simmerling, J. Wang, R. E. Duke, R. Luo, R. C. Walker, W. Zhang, K. M. Merz, B. Roberts, B. Wang, S. Hayik, A. Roitberg, G. Seabra, I. Kolossváry, K. F. Wong, F. Paesani, J. Vanicek, X. Wu, S. R. Brozell, T. Steinbrecher, H. Gohlke, Q. Cai, X. Ye, J. Wang, M.-J. Hsieh, G. Cui, D. R. Roe, D. H. Mathews, M. G. Seetin, C. Sagui, V. Babin, T. Luchko, S. Gusarov, A. Kovalenko and P. A. Kollman AMBER 11, 2010, University of California, San Francisco, CA, USA.
12. (*a*) J. Wang, R. M. Wolf, J. Caldwell, P. A. Kollman and D. A. Case, *J. Comput. Chem.* 2004, **25**, 1157-1174. (*b*) J. Wang, P. A. Kollman and D. A. Case, *J. Mol. Graph. Model.* 2006, **25**, 247-260.
13. W. L. Jorgensen, J. Chandrasekhar, J. D. Madura, R. W. Impey and M. L. Klein, *J. Chem. Phys*. 1983, **79**, 926-935.
14. J.-P. Ryckaert, G. Ciccotti and H. J. C. Berendsen, *J. Comput. Phys.* 1977, **23**, 327-341.
15. R. J. Loncharich, B. R. Brooks and R. W. Pastor, *Biopolymers* 1992, **32**, 523-535.
16. A. Toukmaji, C. Sagui, J. Board and T. Darden, *J. Chem. Phys.* 2000, **113**, 10913-10927.
17. P. Español and P. Warren, *Europhys. Lett.* 1995, **30**, 191-196.
18. R. D. Groot *J. Chem. Phys*. 2003, **118**, 11265-11277.
19. (*a*) P. Posocco, M. Fermeglia and S. Pricl, *J. Mater. Chem.* 2010, **20**, 7742-7753. (*b*) M. Fermeglia and S. Pricl, *Comput. Chem. Eng.* 2009, **33**, 1701-1710. (*c*) R. Toth, D.-J. Voorn, J.-W. Handgraaf, J. G. E. M. Fraaije, M. Fermeglia, S. Pricl and P. Posocco, *Macromolecules* 2009, **42**, 8260-8270. (*d*) G. Scocchi, P. Posocco, A. Danani, S. Pricl and M. Fermeglia, *Fluid Phase Equilibria* 2007, **261**, 366-374.
20. (a) M. Fermeglia, M. Ferrone and S. Pricl, *Fluid Phase Equilib.* 2003, **212**, 315–329. (b) R. Toth, A. Coslanich, M. Ferrone, M. Fermeglia, S. Pricl, S. Miertus and E. Chiellini, *Polymer* 2004, **45**, 8075–8083. (c) M. Fermeglia, M. Ferrone and S. Pricl, *Mol. Simul.* 2004, **30**, 289–300.
21. D. J. Welsh, P. Posocco, S.Pricl and D. K. Smith, *Org. Biomol. Chem.* 2013,**11**, 3177-3186.
22. X. Fan, N. Phan-Thien, S. Chen, X. Wu, T. Y. Ng, *Phys. Fluids* 2006, **18**, 63102-63110.

23. A. Barnard, P. Posocco, S. Pricl, M. Calderon, R. Haag, M. E. Hwang,V. W. T. Shum, D. W. Pack, and D. K. Smith, *J.Am. Chem. Soc.* 2011, **133**, 20288-20300.
24. S. E. Feller, Y. Zhang, R. W. Pastor, and B. R. Brooks, *J. Chem. Phys*. 1995, **103**, 4613-4621.
25. Y. Duan, C. Wu, S. Chowdhury, M. C. Lee, G. M. Xiong, W. Zhang, R. Yang, P. Cieplak, R. Luo, T. Lee, J. Caldwell, J. Wang and P. Kollman, *J. Comput. Chem.*, 2003, **24**, 1999–2012.
26. J. Srinivasan, T. E. Cheatham, P. Cieplak, P. A. Kollman and D. A. Case, *J. Am. Chem. Soc.* 1998, **120**, 9401-9409.
27. V. Tsui and D. A. Case, *Biopolymers* 2000, **56**, 275-291.